POLARIMETRIC RADAR INTERFEROMETRY: A NEW SENSOR FOR VEHICLE BASED MINE DETECTION

Shane R Cloude [1], Chris Thornhill [2]

[1]Applied Electromagnetics
83 Market St., St Andrews
Fife, Scotland, KY16 9NX, UK
[2]DERA Malvern
St. Andrews Rd.
Great Malvern, WR14 3PS,UK

INTRODUCTION

A key challenge in remote mine detection[1] is the ability to detect shallow buried targets in a forward looking geometry. In this paper we investigate the application of a new technique called polarimetric radar interferometry [2,3] . The problem of forward mine detection using radar poses several technical challenges. The first is detection of the small backscatter signal level, which results from the large signal loss due the air/ground interface and to propagation losses in the dielectric soil medium. A second problem is that the surface itself is seldom smooth on the radar wavelength scale and so scattering by surface clutter can dominate the return. Polarimetric Interferometry overcomes these problems by combining two important physical identifying characteristics of a buried target:

- Both the coupling of energy into the ground and the scattering by the target are polarisation dependent [1,4]. The first results from the Fresnel equations which show better coupling for polarisation in the plane of incidence than perpendicular. The second results from the fact that many mines of interest have plastic casings with minimal metal content and so the backscatter signal is dominated by internal waves inside the mine. Since these involve reflection and scattering from dielectric materials, they too depend on the polarisation of the incident wave [1].
- Interferometry is a two antenna array technique whereby the phase difference between elements of the array depends on the position of the phase centre of the target[5]. For buried mine detection the phase centre of the target is separated from the surface (by the optical depth of the target). Hence interferometric phase can be used to separate targets and hence reduce clutter.

Polarimetric Interferometry works by combining these two techniques such that an interferometer measures the phase between all possible polarisation combinations and selects those combinations which maximise the separation of target from clutter. An algorithm for adaptively performing this separation has recently been developed [2,3].

FORMULATION OF THE PROBLEM

Figure 1 shows the basic geometry of a Radar Polarimetric Interferometer. Two measurement positions, 1 and 2 are separated by a physical baseline B. Radar measurements of the full coherent scattering matrix [S] are made at each position in the range/cross range co-ordinate system m/n. By coherently combining signals from 1 and 2, the range difference Δ may be sensed as a phase shift between the signals. By transforming the data into the surface x/y co-ordinate (through a process called range filtering[5]) the sensor can be used to locate the z co-ordinate of a scattering point.

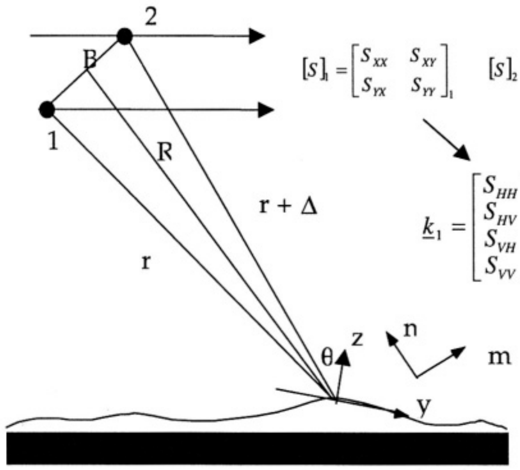

$$[S]_1 = \begin{bmatrix} S_{XX} & S_{XY} \\ S_{YX} & S_{YY} \end{bmatrix}_1 \qquad [S]_2 = \begin{bmatrix} S_{XX} & S_{XY} \\ S_{YX} & S_{YY} \end{bmatrix}_2$$

$$\underline{k}_1 = \begin{bmatrix} S_{HH} \\ S_{HV} \\ S_{VH} \\ S_{VV} \end{bmatrix}_1 \qquad \underline{k}_2 = \begin{bmatrix} S_{HH} \\ S_{HV} \\ S_{VH} \\ S_{VV} \end{bmatrix}_2$$

$$[P] = \left\langle \begin{bmatrix} \underline{k}_1 \\ \underline{k}_2 \end{bmatrix} \cdot \begin{bmatrix} \underline{k}_1^{*T} & \underline{k}_2^{*T} \end{bmatrix} \right\rangle = \begin{bmatrix} T_{11} & \Omega_{12} \\ \Omega_{12}^{*T} & T_{22} \end{bmatrix}$$

$$\underline{k} = \begin{bmatrix} a \\ b \\ c \\ d \end{bmatrix} = |\underline{k}| \begin{bmatrix} \cos\alpha e^{i\phi_1} \\ \sin\alpha \cos\beta e^{i\phi_2} \\ \sin\alpha \sin\beta \cos\gamma e^{i\phi_3} \\ \sin\alpha \sin\beta \sin\gamma e^{i\phi_4} \end{bmatrix} = |\underline{k}|\ \underline{w}$$

$$\left.\begin{array}{l} \mu_1 = \underline{w}_1^{*T} \underline{k}_1 \\ \mu_2 = \underline{w}_2^{*T} \underline{k}_2 \end{array}\right\} \Rightarrow \mu_1 \mu_2^* = \begin{cases} \gamma = \dfrac{|\langle \mu_1 \mu_2^* \rangle|}{\sqrt{\langle \mu_1 \mu_1^* \rangle \langle \mu_2 \mu_2^* \rangle}} & \text{coherence } 0 \le \gamma \le 1 \\ \phi = \arg\left(\underline{w}_1^{*T} \Omega_{12} \underline{w}_2\right) & \text{interferometric phase } \phi \end{cases}$$

Figure 1 : Basic Geometry and Equations of Polarimetric Radar Interferometry

In order to analyse such problems we employ a coherency matrix formalism so as to maintain phase shifts between all polarisation channels. This requires generation of a 2N x 2N coherency matrix from the original N x N polarimetric problem. Figure 1 shows how this matrix can be defined from the polarimetric scattering vectors from each end of the baseline. The hermitian matrix [P] may be factored into three N x N block matrices as shown. The matrices $[T_{11}]$and $[T_{22}]$ are the conventional polarimetric coherency matrices. The matrix $[\Omega_{12}]$ is a complex N x N matrix which contains the relative phase information about the structure of the scattering volume.

In order to extract information from this matrix, use is made of a scalar parameter, the interferometric coherence γ, defined in figure 1. Here we show from left to right how a vector interferogram can be formed for arbitrary scattering mechanisms[2] $\underline{w}_1$ and $\underline{w}_2$. The scattering mechanism $\underline{w}$ is defined as a normalised scattering vector as shown. The coherence γ is a function of the choice of filter $\underline{w}$. Hence, if we can find a $\underline{w}$ for which $\gamma =$ 1, then we have successfully isolated a scattering centre in the volume which has a well defined phase centre. Hence maximising $\gamma(\underline{w})$ is a clear objective in determining structure within the scattering volume. It has been shown [3] that the $\underline{w}$ vectors which maximise the coherence are given as solutions of an eigenvalue problem. There are N such maxima, given by vectors $\underline{w}_1$ and $\underline{w}_2$ which are solutions of the following equations

$$\begin{aligned} T_{22}^{-1}\Omega_{12}^{*T}T_{11}^{-1}\Omega_{12}\underline{w}_2 &= \lambda\underline{w}_2 \\ T_{11}^{-1}\Omega_{12}T_{22}^{-1}\Omega_{12}^{*T}\underline{w}_1 &= \lambda\underline{w}_1 \end{aligned} \qquad \lambda = \gamma_{opt}^2 \in \Re \qquad \text{- 1)}$$

Sub-Clutter Visibility Using Polarimetric Interferometry

Consider the problem of finding a target embedded in a clutter background. We assume that the target has rotation symmetry (like a plastic mine) so that it generates zero cross-polarisation. In this case the polarimetric coherency matrix is 2 x 2 (only HH and VV are significant). Hence N = 2 and the matrix [P] is 4 x 4 hermitian. The filter $\underline{w}$ then has only two parameters α,δ as shown in equation 2

$$\underline{w} = \begin{bmatrix} \cos\alpha \\ \sin\alpha e^{i\delta} \end{bmatrix} \qquad \text{- 2)}$$

Another way to view the role of the coherence optimiser in polarimetric interferometry is to consider it as a contrast optimisation procedure. In this way the target is defined as the scattering mechanism $\underline{w}$ which has the best phase centre in the data (a mine target for example) and the clutter becomes everything else (surface clutter, vegetation etc). The contrast optimisation can then be represented by the following related matrix eigenvalue equation

$$T_{clutter}^{-1}T_{target}\underline{w} = \lambda\underline{w} \qquad \text{- 3)}$$

where the eigenvectors $\underline{w}$ are the scattering mechanisms which maximise the signal to clutter ratio between the two processes with polarimetric coherency matrices T_{target} and $T_{clutter}$. The eigenvalues λ are the values of the optimum contrast and hence are important in estimating the sub-clutter visibility. The important point to note is that the vectors $\underline{w}$ which satisfy equation 3 also satisfy the optimiser equation 1.

In general terms we can then write the two hermitian coherency matrices, one for the clutter and one for the target in terms of their eigenvalue decompositions so that

$$\left.\begin{aligned} T_{target} &= \lambda_t\underline{e}_1\underline{e}_1^{*T} + \varepsilon\underline{e}_2\underline{e}_2^{*T} \\ T_{clutter}^{-1} &= \frac{1}{\lambda_c}\underline{e}_3\underline{e}_3^{*T} + \frac{1}{\varepsilon}\underline{e}_4\underline{e}_4^{*T} \end{aligned}\right\} \quad \varepsilon = \text{noise or depolarisation level} \qquad \text{- 4)}$$

Where

- λ_t is the target scattering cross section
- λ_c is the clutter cross section
- ε is the system noise level, which will either be set by the thermal noise or by noise generated by depolarisation of the signal by the clutter.
- $\underline{e}_1, \underline{e}_2$ are orthogonal independent scattering mechanisms for the target
- $\underline{e}_3, \underline{e}_4$ are orthogonal independent scattering mechanisms for the clutter

Note that $\underline{e}_3, \underline{e}_4$ are independent of $\underline{e}_1, \underline{e}_2$. The contrast optimisation can then be written from equation 3 in the form shown in figure 2.

$$T_{clutter}^{-1}\; T_{t\arg et} = \frac{\lambda_t}{\lambda_c}\left(m_{13}\, \underline{e}_1 \underline{e}_3^{*T} + \frac{\varepsilon}{\lambda_t} m_{32}\, \underline{e}_3 \underline{e}_2^{*T} + \frac{\lambda_c}{\varepsilon} m_{14}\, \underline{e}_1 \underline{e}_4^{*T} + \frac{\lambda_c}{\lambda_t} m_{42}\, \underline{e}_4 \underline{e}_2^{*T} \right)$$

$$m_{ij} = \underline{e}_i^{*T}\, \underline{e}_j$$

$$\boxed{\text{Contrast} = \text{S/C} + \text{C/N} + \text{G}_\text{p}} \qquad Contrast = \frac{\lambda_t}{\lambda_c} \cdot \frac{\lambda_c}{\varepsilon} . m_{14}$$

Figure 2 : Definition of Target Contrast

Note that there are four terms in the expansion. The whole expression is multiplied by a common factor, which is the raw signal-to-clutter ratio. In practice this may be around 0 dB or worse (some indications for buried plastic mines in surface clutter are around –16 dB S/C ratio). Of the four terms inside the expansion, three have order unity or zero while the highlighted third term will generally be dominant and can provide processing gain. For clarity we have isolated this component and expressed it as the product of three significant terms. It is the net product of these terms (called the contrast) that can provide the gain in sub-clutter visibility using polarimetric interferometry. The three terms are:

- S/C ratio of the raw data
- C/N which is the effective clutter to noise ratio of the system
- G_p, the polarimetric gain. The factor m_{14} is the projection of the target scattering mechanism onto the orthogonal clutter space.

This projection term G_p can be 0 dB maximum, in which case we can recover a maximum factor equal to the C/N ratio (which can be very substantial). In the worst case however, $m_{14} = 0$ (if $\underline{e}_1 = \underline{e}_3$ for example) and we lose any discrimination capability between the clutter and target, We now try and estimate these factors for the problem of wide band detection of buried mine targets.

Buried Mine Detection Using Polarimetric Interferometry

The problem to be considered is shown in figure 3. Here we see a buried mine target at depth d below a surface interface. The radar system illuminates the surface at an angle θ and the soil has a dielectric constant ε_r which may be complex. The problem has three important components as shown in figure 3.

- The clutter matrix is assumed to be given by a backscatter polarimetric surface model[6]. Hence the coefficients A, B and C are assumed to be Bragg scattering coefficients while the parameter β indicates surface roughness. We shall use rough surface backscatter data from the JRC EMSL facility to estimate the parameters

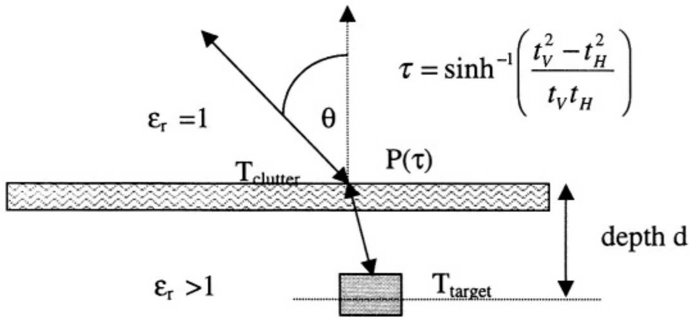

$$T_g^{-1}T_t = \frac{1}{d}\begin{bmatrix} \frac{C_g}{2}(1+\sin c4\beta) & -B_g \sin c2\beta \\ -B_g \sin c2\beta & A_g \end{bmatrix}\begin{bmatrix} \cosh\tau & \sinh\tau \\ \sinh\tau & \cosh\tau \end{bmatrix}\cdot\begin{bmatrix} A_t & B_t \\ B_t^* & C_t \end{bmatrix}\cdot\begin{bmatrix} \cosh\tau^* & \sinh\tau^* \\ \sinh\tau^* & \cosh\tau^* \end{bmatrix} \qquad -5)$$

JRC EMSL Data FDTD Simulation

Figure 3 : Geometry of Buried Mine Detection Problem

- The coupling of energy through the air/ground interface can be represented as a diattenuation i.e. as a polarisation dependent attenuation of the incident signal. The coupling is given by the Fresnel equations, which depend on the angle of incidence and on the dielectric constant ε_r. The diattenuation parameter τ is a function of the ratio of these parameters as shown in figure 3. The effect of the surface on the detection performance is modelled by a matrix product as shown in equation *5*.

- The backscattering from the target embedded in a dielectric background must be obtained through numerical modelling. For plastic mine targets, energy is coupled inside the mine and is reflected and scattered from internal dielectric surfaces. These processes are frequency and polarisation dependent and hence a UWB interrogation pulse is used to obtain the spectral target signature. We used a finite difference time domain (FD-TD) model of a typical plastic anti tank mine target,.

At shallow angles the Bragg backscatter yields small α angles for the surface[6]. However, the target also has small α values and so the projection of the target onto the orthogonal clutter space is small. Hence the gain is small, around –10 dB or less. However, as long as the C/N ratio is better than this figure, then some sub-clutter visibility will be obtained. At steeper angles the projection of the target onto the orthogonal clutter space improves and the polarimetric gain increases. Here the gain can be around –2 dB at certain frequencies. Hence we might conclude that steeper angles of incidence would provide improved sub-clutter visibility and hence better detection of buried mines. However there is one counter argument to this. The problem is that the C/N ratio has two components. The first is the system noise floor which is independent of angle of incidence. The second is the depolarisation by the surface. To illustrate the problem we consider the 2 x 2 surface clutter matrix. Its dominant eigenvector will be a Bragg surface component. However, its second eigenvalue will not generally be zero, due for example to surface roughness causing depolarisation (the β parameter in figure 3). In this case the effective C/N ratio must be defined as the ratio of eigenvalues of the clutter matrix as shown in equation 7

$$\begin{bmatrix} \langle hh \rangle^2 & \langle hhvv^* \rangle \\ \langle vvhh^* \rangle & \langle vv \rangle^2 \end{bmatrix} = [U_2] \begin{bmatrix} \lambda_a & 0 \\ 0 & \lambda_b \end{bmatrix} [U_2]^{*T} \Rightarrow \frac{C}{N} = -10\log\frac{\lambda_b}{\lambda_a} \qquad -7)$$

The problem is that this C/N ratio is a function of θ and generally the surface depolarisation increases with θ, so acting to counter the increasing G_p with θ.

We have used the JRC-EMSL surface scattering data to estimate the C/N ratio. We found that for shallow angles the C/N ratio is good (around 25 dB which, in combination with figure 11, gives a sub-clutter visibility around 15 dB). However, at steeper angles this C/N ratio falls to around 12 dB (which corresponds to a sub-clutter visibility of around 10 dB). Hence, although the G_p factor improves with θ, the effective sub-clutter visibility does not vary very much with θ. It does seem however that around 10-15 dB of sub-clutter visibility could be obtained from such a sensor.

SIMULATION RESULTS FOR UWB VEHICLE BASED SYSTEM

To illustrate the above concepts, consider the problem of finding two targets located 15m in front of the vehicle. We assume they are separated by 30cm depth and the S/C ratio is –14dB in HH and –8dB in VV. Figure 4 shows the raw data obtained from sensor positions 1 and 2. The radiated pulse is the derivative of a Gaussian with FWHH = 100ps and we have a good S/N ratio of 50 dB.

Figure 4 also shows the interferometric coherence and phase, averaged over a decade of bandwidth. The x-axis is obtained by first time shifting one channel relative to the other to scan in depth for the targets. We see that in both the HH and VV channels, the main target has been found (a target is located if its coherence is 1 **and** its phase is zero)

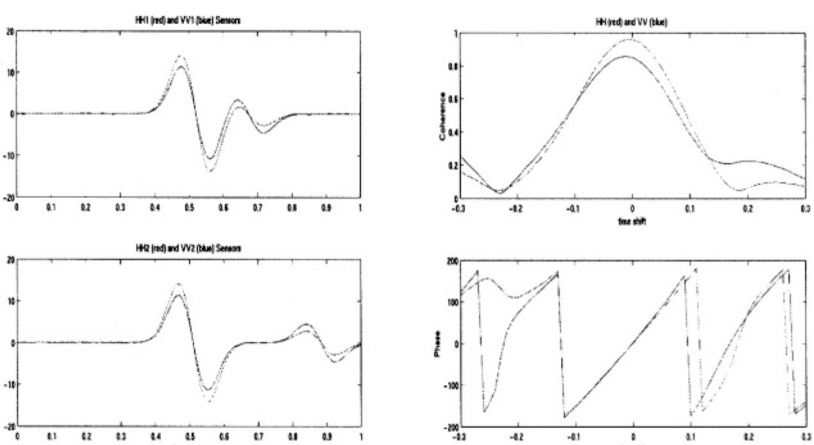

Figure 4 : Simulations of Buried target in Clutter (Raw Time Domain Signals (left) and Interferometric Coherence and Phase (right)

However, there is no indication of the second target since the coherence estimation is dominated by the larger signal from the 'clutter'. It is here that polarimetry plays an important role. Figure 5 shows the results of using the coherence optimiser (equation 1) on the same data to obtain the maximum coherence and corresponding phase of the combined signals. Here we see a kind of super-resolution. In this case the optimiser again finds the main surface component at zero shift. However to the left and right it also finds local maxima in the coherence. These correspond to possible secondary targets. The one to the right however has a phase larger than zero and corresponds to a coupling of the surface target from position 1 with the buried target from position 2. However, the phase of this cross term will never be zero (unless the two targets are identical). The maximum to the left corresponds to our desired second target. It has zero phase (i.e. it is the same target from baseline 1 and 2) and it has high coherence. Figure 5 also shows the α value selected by the optimiser. The surface clutter has a scattering mechanism with $\alpha = 39°$. Hence its orthogonal sub-space has $\alpha = 51°$. We see that the optimiser moves into this sub-space as we shift away from zero time shift. This confirms its ability to adapt to the local polarimetric properties of the target.

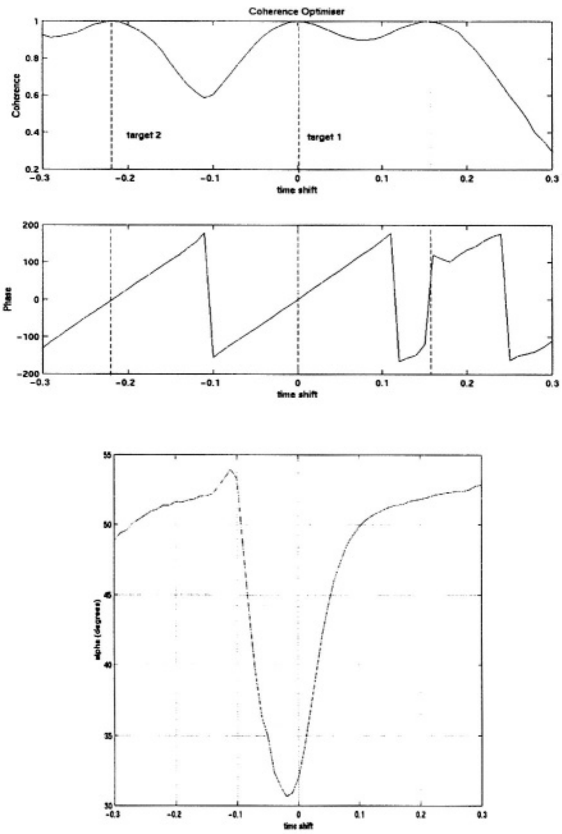

Figure 5 : Optimum Coherence and Phase (top) and α parameter of the optimiser (bottom)

EXPERIMENTAL RESULTS FOR VEHICLE BASED UWB RADAR SYSTEM

In order to investigate the feasibility of employing polarimetric interferometry from a vehicle, DERA Malvern have developed an array system mounted on a landrover platform. In this way coherent wide band data can be collected at HH and VV polarisations from either end of a baseline. Figure 6 shows sample experimental results for a calibration sphere located on the surface in front of the vehicle (the surface is located at zero time shift in figure 6). The coherences were calculated over a decade of bandwidth from 0.3 – 3GHz.

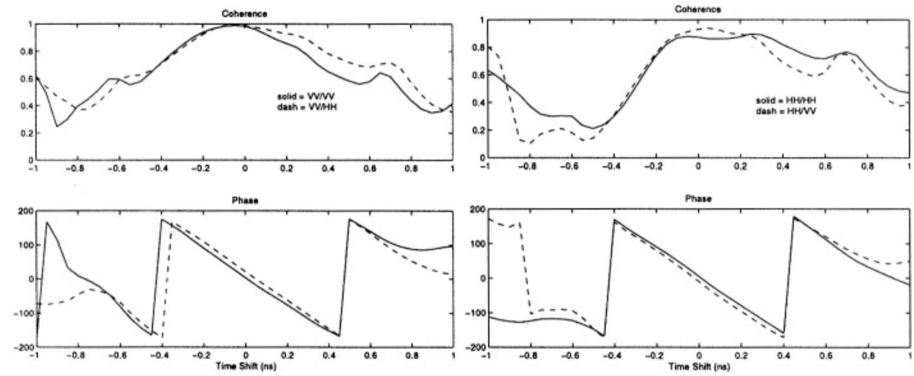

Figure 6 : Coherence/Phase Plots for Experimental Data Collected for 30cm sphere target by DERA Vehicle System

Also shown are phase plots indicating the precise location of the target at the zero phase crossings. We conclude that high coherence can be obtained and precise vertical localisation achieved in all polarisation channels. The results demonstrate the basic feasibility of employing such methods for the detection and location of targets in forward looking geometries. Future studies will address the detection of buried targets.

Acknowledgements

The authors gratefully acknowledge the support of the Defence Evaluation and Research Agency, DERA Malvern, UK.

REFERENCES

[1] "UWB SAR Detection of Dielectric Targets" S. R. Cloude, A. Milne, G Crisp, C Thornhill, Eurel International Conference on the Detection of Abandoned Land Mines, BEE publication No. 431, October 1996, pp 114-118

[2] "Polarimetric SAR Interferometry", S R Cloude, K P Papathanassiou, IEEE Transactions on Geoscience and Remote Sensing, Vol 36. No. 5, pp 1551-1565, September 1998

[3] "Polarimetric Optimisation in Radar Interferometry", S R Cloude, K P Papathanassiou, Electronics Letters, Vol. 33, N0. 13, June 1997, pp 1176-1178

[4] "Polarization Processing for UWB Signals" S.R. Cloude In : Ultra-Wideband Short Pulse Electromagnetics 3, edited by C E Baum, L Carin & A P Stone, Plenum Press 1997, pp 461-468

[5] R. Bamler, P. Hartl, 1998, "Synthetic Aperture Radar Interferometry", Inverse Problems, 14,R1-R54

[6] S R Cloude, I Hajnsek, K P Papathanssiou "An Eigenvector Method for the Extraction of Surface Parameters in Polarimetric SAR", Proceedings of ESA CEOS SAR Workshop, Toulouse, France, October 1999. Paper available at http://www.estec.esa.nl/papers/po26.pdf